Two-quasiparticle K isomers within the covariant density functional theory

Karakatsanis, Konstantinos E.; Lalazissis, G. A.; Prassa, Vaia; Ring, Peter

Two-quasiparticle K isomers within the covariant density functional theory

Konstantinos E. Karakatsanis [1,2,*] G. A. Lalazissis [2] V. Prassa [3] and Peter Ring [4]

[1]*Department of Physics, Faculty of Science, University of Zagreb, HR-10000 Zagreb, Croatia*

[2]*Department of Physics, Aristotle University of Thessaloniki, Thessaloniki GR-54124, Greece*

[3]*Department of Computer Science and Telecommunications, School of Sciences, University of Thessaly, Lamia GR-35100, Greece*

[4]*Department of Physik, Technische Universität München, D-85747 Garching, Germany*

(Received 5 November 2019; revised 23 June 2020; accepted 24 August 2020; published 8 September 2020)

Two-quasiparticle excitations of medium mass nuclei with well-defined axial deformation are studied within the covariant density functional framework. The evolution of high-K isomers is analyzed in a self-consistent axially symmetric relativistic Hartree-Bogoliubov calculation using the blocking approximation. The occurrence of the 6^+ and 8^- low-energy high-K isomers in the region from Er to Pb ($68 \leqslant Z \leqslant 82$, $98 \leqslant N \leqslant 112$) is evaluated and compared to available data. The importance of the quasiparticle spectrum in the energy evolution of the high-K states is discussed in detail.

DOI: 10.1103/PhysRevC.102.034311

I. INTRODUCTION

Nuclear isomers are metastable states of nuclei with half-lifes 100–1000 times longer than normally excited states. As nuclear excited states, they can decay through γ emission, β decay, electron conversion, α decay, or fission. In general, for cases where the nuclear matrix elements of the transition operator are connected with large changes in particular quantum numbers, the corresponding direct decay to the ground state (g.s.) is significantly hindered.

K isomers are a special case of such excitations. They occur in well-deformed heavy nuclei where the angular momentum quantum number K along the symmetry axis plays an important role. More specifically, they are formed as configurations of multiparticle or multiquasiparticle excitations with high-K values. The direct decay to the $K = 0$ ground state involves a large change in K and violates the K-selection rule $\Delta K \leqslant \lambda$. The actual deexcitation follows an alternative path through the rotational bands by an $E1$ or $M1$ transition, and, depending on the energy levels of the rotational states, this leads to a metastable excited state.

The study of isomers, in general, has been an active field of research for many decades. It is a wide subject related to nuclear structure phenomena as well as nuclear reactions. Recent reviews include: the list of all isomers with half-lifes greater than 10 ns by Jain *et al* [1], the connection of shape coexistence and shape isomers by Heyde and Wood [2], the compilation of high-K isomers with mass number $A > 100$ by Kondev *et al* [3]; the discussion by Walker and Xu [4] on K isomers in rotational nuclei, the comprehensive review by Dracoulis *et al* on high-spin isomers for $A > 150$ [5], the summary of recent experimental efforts studying K isomers in superheavy nuclei by Ackermann [6] and Ackermann and Theisen [7], and the most recent historical outline of nuclear isomer research by Walker and Podolyák [8].

The first theoretical efforts to study isomeric states as multiquasiparticle states in nuclei were based on the Nilsson model [9] with improvements including pairing through the BCS method [10,11], blocking [12,13], and residual interactions between quasiparticles [14,15]. At that time, this model with fixed deformations proved to be very successful in the description of multiquasiparticle states in well-deformed nuclei [12,16–18]. However, later on, it has been recognized, that the polarization induced by the multiquasiparticle configurations changes the deformation of the mean potential [19]: The microscopic-macroscopic method based on the Strutinsky approach [20] has been extended to configuration-constrained energy surface calculations of multiquasiparticle nuclear states. In addition to the Nilsson potential, a deformed Woods-Saxon field was used in many of those applications [21–34]. There are also self-consistent calculations based on nonrelativistic Skyrme [35–42] and Gogny [43–45] functionals. Finally, the covariant density functional approach has also been applied for the study of two-quasiparticle (2qp) excitations in transactinide nuclei [46].

For investigations of rotational bands built on isomeric states, several methods have been used: For strongly deformed axially symmetric configurations, angular momentum projected Hartree-Fock calculations are possible [47–49]. K mixing and alignment processes can be taken into account in the cranked shell model. Its original version [50] uses a constant pairing gap, but there are also self-consistent relativistic cranked Hartree-Bogoliubov calculations in Ref. [51]. However, because of the blocking phenomena for the various quasiparticle configurations, pairing correlations have been treated in a more sophisticated way, e.g., by number projection or by an exact diagonalization of the pairing interaction within the pairing window [52–56]. The projected shell model of Hara and Sun [57] allows K mixing as well as exact angular

*kokaraka@auth.gr

momentum projection. It has been used for the investigation of K isomers in Refs. [58–61]. More details on the historical evolution of these approaches and their extended applications to K isomers can be found in Ref. [4].

The present paper focuses on a fully self-consistent systematic study of K isomers, which arise as multiquasiparticle excitations of the nuclear ground state. High-K isomers in well-deformed axially symmetric even-even nuclei with $A > 100$ are investigated within the self-consistent relativistic-Hartree-Bogoliubov (RHB) framework using the blocking approximation [62]. In contrast to many of the investigations cited above, where specific parameters of the models have been adjusted to some data, all the results of this investigation are derived from two well-known and very successful universal covariant density functionals, adjusted in the literature more than a decade ago to ground-state properties of even-even nuclei. We focus on nuclei with well-established K isomers in the region of Hf and Er isotopes and on K isomers in the ($A \approx 180$) region [63,64] where there has been recently great experimental effort to study their existence [3].

The paper is organized in the following order. The theoretical framework and the formation of isomers is described in Sec. II. In order to outline the importance of the single-particle evolution in the formation of high-K isomers, in Sec. III, the Nilsson diagrams for ^{176}Hf are discussed. In Sec. IV, we study the influence of pairing correlations. The results of the theoretical calculations are presented in Sec. V. Specifically, the evaluation of the 6^+ and 8^- high-K isomers in Hf isotopes and $N = 104$ and $N = 106$ isotones are compared to data. Section VI summarizes our main conclusions.

II. THEORETICAL FRAMEWORK

One of the most successful theoretical frameworks for studies of nuclear structure phenomena is based on concepts of nonrenormalizable effective relativistic field theories and density functional theory (DFT).

This approach provides a microscopically consistent but still simple and economical treatment of the nuclear many-body problem. By adjusting just a few model parameters to global properties of spherical and stable nuclei, it is possible to describe in detail a variety of nuclear structure phenomena over the entire periodic table. At present, all successful nuclear energy density functionals are based on phenomenology and symmetries play an essential role.

One of the underlying symmetries of QCD is Lorentz invariance and, therefore, covariant density functionals (CDF) [65–67] are of particular interest in nuclear physics. They exploit basic properties of QCD at low energies, in particular, symmetries and the separation of scales [68]. Within the CDF realization, the spin degree of freedom is taken into account consistently. The complicated interplay between the large Lorentz scalar and the vector self-energies which, on the QCD level, can be understood by the in medium changes in the scalar and vector quark condensates [69] is included in a self-consistent way. The nuclear currents induced by the spatial parts of the vector self-energies are taken into account. These currents play an essential role in the description of rotating nuclei [70] and in the description of the magnetic moments of single-particle configurations [71]. At present, all attempts to derive these functionals directly from the bare nucleon-nucleon forces do not reach the required accuracy [72]. In recent years, universal covariant density functionals have been derived by fine-tuning a few phenomenological parameters to properties of nuclear matter and finite nuclei. They provide an excellent description of ground-state and excited-state properties of nuclei all over the periodic table with a high predictive power [73–76].

Most applications of the RMF theory were restricted to meson-nucleon models of nuclear dynamics in which the couplings between nucleon densities are mediated by finite-range meson propagators. Modern versions of such models use density-dependent coupling constants as, for instance, the parameter set DD-ME2 [73]. This density functional has been used with great success for investigations of ground states and excited states in nuclei all over the periodic table. The point coupling models with zero-range interactions present an interesting alternative to the meson-nucleon models. Recently, the set DD-PC1 [74] has been adjusted to nuclear matter data and to masses of a series of deformed nuclei. In principle, these two types of models should be equivalent since the expansion of the meson propagator yields a zero-range coupling plus derivative corrections. Therefore, the point coupling model should also provide a very good description of low-energy nuclear structure phenomena. Also, the numerical implementation of the point coupling models is much simpler than that of the meson-nucleon models, and the calculations involved are far less time consuming. Within the proposed investigations, we use both parameter sets and compare their results.

Nuclei with open shells show a superfluid behavior and, therefore, pairing correlations are also important. In density functional theory, they are taken into account by means of a generalized Slater determinant $|\Phi\rangle$ of the Hartree-Bogoliubov type. In that framework, the nuclear ground-state $|\Phi\rangle$ is represented as the *vacuum* with respect to independent quasiparticles, which is the basic concept introduced in the mean-field approximation to deal with both long-range particle-hole correlations and short-range particle-particle correlations at the same time. Quasiparticles are defined by a unitary linear transformation from the particle c_l^+, c_l creation and annihilation operators,

$$\alpha_k^+ = \sum_l U_{lk} c_l^+ + V_{lk} c_l, \tag{1}$$

or in matrix form

$$\begin{pmatrix} \alpha \\ \alpha^+ \end{pmatrix} = \begin{pmatrix} U^+ & V^+ \\ V^T & U^T \end{pmatrix} \begin{pmatrix} c \\ c^+ \end{pmatrix} = \mathcal{W}^+ \begin{pmatrix} c \\ c^+ \end{pmatrix}, \tag{2}$$

where α_k^+, α_k are the corresponding creation and annihilation operators for quasiparticles and $\mathcal{W}$ is the unitary matrix of the transformation. The Hartree-Bogoliubov coefficients U_{lk}, V_{lk} completely determine the total wave function of the nuclear many-body system. They also determine the Hermitian single-particle density matrix,

$$\hat{\rho} = V^* V^T, \tag{3}$$

and the antisymmetric pairing tensor or abnormal density,

$$\hat{\kappa} = V^* U^T. \tag{4}$$

The energy density functional contains *ph* terms derived from a Lorentz-covariant Lagrangian, corresponding to a specific functionals, such as the DD-ME2 and DD-PC1, and *pp* terms produced by effective nonrelativistic forces. Therefore, the energy functional depends not only on the density-matrix $\hat{\rho}$ and the meson fields ϕ_m, but also on the pairing tensor,

$$E[\hat{\rho}, \hat{\kappa}, \phi_m] = E_{\rm RMF}[\hat{\rho}, \phi_m] + E_{\rm pair}[\hat{\kappa}], \tag{5}$$

where $E_{\rm RMF}[\hat{\rho}, \phi]$ is the RMF functional. The pairing energy $E_{\rm pair}[\hat{\kappa}]$ is given by

$$E_{\rm pair}[\hat{\kappa}] = \tfrac{1}{4}{\rm Tr}[\hat{\kappa}^* V^{pp} \hat{\kappa}]. \tag{6}$$

V^{pp} is a general two-body interaction that, in the present paper, corresponds to the pairing part of the well-known Gogny interaction [77]. In order to simplify the numerical calculations, we use, here, the separable Tian-Ma-Ring (TMR) pairing force of Refs. [78,79]. It is adjusted to the pairing properties of the Gogny force in nuclear matter and in all practical applications equivalent to it.

The minimization of the energy functional through a variation with respect to the density matrix and pairing tensor leads to the corresponding RHB equations [80],

$$\begin{pmatrix} \hat{h}_D - \lambda & \hat{\Delta} \\ -\hat{\Delta}^* & -\hat{h}_D + \lambda \end{pmatrix} \begin{pmatrix} U_k(\boldsymbol{r}) \\ V_k(\boldsymbol{r}) \end{pmatrix} = E_k \begin{pmatrix} U_k(\boldsymbol{r}) \\ V_k(\boldsymbol{r}) \end{pmatrix}. \tag{7}$$

The self-consistent mean field is the Dirac Hamiltonian $\hat{h}_D$, and it includes all the long-range particle-hole (*ph*) correlations and is defined by

$$\hat{h}_D = \frac{\delta E}{\delta \hat{\rho}}. \tag{8}$$

For meson exchange models, this takes the form

$$h_D(\boldsymbol{r}, \boldsymbol{r'}) = \boldsymbol{\alpha} \cdot \boldsymbol{p} + V(\boldsymbol{r}) + \beta[M + S(\boldsymbol{r})], \tag{9}$$

where the scalar and vector potentials,

$$S(\boldsymbol{r}) = g_\sigma \sigma(\boldsymbol{r}), \tag{10}$$

$$V(\boldsymbol{r}) = g_\omega \omega^0 + g_\rho \tau_3 \rho^0(\boldsymbol{r}) + e\frac{1-\tau_3}{2} A^0(\boldsymbol{r}) \tag{11}$$

depend on the scalar meson σ and the timelike components ω^0, ρ^0, and A^0 of the isoscalar vector meson ω, the isovector vector meson ρ, and the electromagnetic-field A. The spacelike components are neglected because of the time-reversal symmetry.

The pairing field $\hat{\Delta}$, describes the particle-particle (*pp*) correlations,

$$\hat{\Delta} = \frac{\delta E}{\delta \hat{\kappa}}. \tag{12}$$

The subsidiary condition on the particle number determines the chemical potential λ so that the particle number operator has an expectation value in the ground state equal with the number of nucleons. The quasiparticle wave functions are completely determined by the coefficients U_k and V_k with the respective quasiparticle energies E_k. The RHB matrix has dimension $M = 2N$, twice that of the corresponding Dirac equation. Thus, for every eigenvector (U_k, V_k) with positive quasiparticle energy $E_k > 0$, corresponds to an eigenvector (V_k^*, U_k^*) with quasiparticle energy $-E_k$. Since the baryon quasiparticle operators satisfy fermion commutation relations, the levels with E_k and $-E_k$ cannot be occupied simultaneously. For the solution that corresponds to the ground state of a nucleus with even particle number, one usually chooses the eigenvectors with positive eigenvalues E_k. A detailed discussion on the numerical application of the described theoretical framework can be found in Ref. [81].

A. Isomer formation

K isomers are a special case of single-particle low-lying nuclear excitations. They appear in many well-deformed heavy nuclei, where K, the projection of the total angular momentum **J** onto the symmetry axis, is approximately a good quantum number. Their formations originate by the fact that, in certain regions of the periodic table, orbitals with high values of single-particle angular momentum j come close to the Fermi surface. Thus, with a minimal amount of energy which is roughly equal as the energy required to break the required number of nucleon pairs, it is possible to create excited states of two or more quasiparticles, involving configurations of such orbitals. For a combination of n quasiparticles, the resulting nucleus is one of the 2^{n-1} multiplet excited states with total K and parity, determined by the combination of the individual quasiparticle orbitals as follows:

$$K = |\pm K_1 \pm K_2 \pm \cdots \pm K_n|, \quad \pi = \prod^n \pi_i. \tag{13}$$

Typically, among those states, the one with the highest value of K, $K = \sum_i |K_i|$ has the lowest energy and is the best candidate for an actual K isomer.

In order to study K-isomeric excitations, we use the blocking effect within the Hartree-Bogoliubov framework to create multiquasiparticle states starting from the ground-state $|\Phi_0\rangle$ of a system under investigation. This ground state is defined as the quasiparticle vacuum, i.e.,

$$\alpha_k|\Phi_0\rangle = 0 \quad \text{for} \quad E_k > 0 \quad \text{or} \quad |\Phi_0\rangle = \prod_{E_k>0} \alpha_k|-\rangle, \tag{14}$$

where $|-\rangle$ is the bare vacuum of the configuration space defined by the original single particles. If $|\Phi_0\rangle$ describes an even system as is usually the case, one can study the neighboring odd system by constructing a one-quasiparticle state $|\Phi_1\rangle$,

$$|\Phi_1\rangle = \alpha_1^\dagger|\Phi_0\rangle = \alpha_1^\dagger \prod_k \alpha_k|-\rangle, \tag{15}$$

by blocking the quasiparticle state with the lowest energy, which corresponds to the operator $\alpha_1^\dagger$. This is performed, for example, in Ref. [82]. The same procedure can be extended for the low-lying excitations of the even system by constructing, for example, two-quasiparticle states,

$$|\Phi_2\rangle = \alpha_1^\dagger \alpha_2^\dagger|\Phi_0\rangle. \tag{16}$$

The new state represents the vacuum of the set of quasiparticle operators $(\alpha_1', \alpha_2', \ldots, \alpha_N')$ where N is the dimension of the

quasiparticle space with

$$\alpha'_1 = \alpha^\dagger_1, \quad \alpha'_2 = \alpha^\dagger_2, \quad \alpha'_3 = \alpha_3, \ldots, \alpha'_N = \alpha_N. \tag{17}$$

In this way, a new quasiparticle basis is defined by the set of operators $(\alpha'_1, \ldots, \alpha'_N, \alpha'^\dagger_1, \ldots, \alpha'^\dagger_N)$ where we have exchanged operators $\alpha^\dagger_1 \leftrightarrow \alpha_1$ and $\alpha^\dagger_2 \leftrightarrow \alpha_2$ which is equivalent to the exchange of the columns $(U_{l1}, V_{l1}) \leftrightarrow (V^*_{l1}, U^*_{l1})$ and $(U_{l2}, V_{l2}) \leftrightarrow (V^*_{l2}, U^*_{l2})$ in the transformation matrix $\mathcal{W}$ in Eq. (2). In other words, in order to study the lowest-lying excitations applying the blocking effect, one needs to exchange the annihilation operators α_1, α_2 with the creation operators $\alpha^\dagger_1$, $\alpha^\dagger_2$ corresponding to the quasiparticle states with the lowest energies, or in the single-particle basis to the states that are closer to the Fermi surface.

In practice, this means that, by blocking the orbit k_b, we have to replace, in Eqs. (3) and (4), the densities ρ and κ by

$$\rho_{k_b} = \rho + \left(U_{k_b} U^{*T}_{k_b} - V^*_{k_b} V^T_{k_b}\right), \tag{18}$$

$$\kappa_{k_b} = \kappa + \left(U_{k_b} V^{*T}_{k_b} - V^*_{k_b} U^T_{k_b}\right), \tag{19}$$

where U_{k_b} and V_{k_b} correspond to the Bogoliubov coefficients U and V of the blocked quasiparticle level. By this definition, their nucleon-pair $(k_b, -k_b)$ is broken, and it does not contribute to the pairing tensor. The blocked wave-function $|\Phi_{k_b}\rangle = \alpha^\dagger_{k_b}|\Phi_0\rangle$ as well as $|\Phi_{-k_b}\rangle = \alpha^\dagger_{-k_b}|\Phi_0\rangle$ do not obey time-reversal symmetry, and this leads to currents around the symmetry axis. The current in the blocked states $|\Phi_{k_b}\rangle$ and $|\Phi_{-k_b}\rangle$ have opposite directions.

Blocking two-quasiparticle states k_b and k'_b in different pairs leads in analogy to Eqs. (18) and (19) to the densities ρ_{k_b,k'_b} and κ_{k_b,k'_b} which break time-reversal symmetry.

In a first step, we conserve time-reversal symmetry for the blocked states. This is performed within the equal filling approximation (EFA) in the Hartree-Fock-Bogoliubov (HFB) framework [83] by averaging over the densities ρ_{k_b} and ρ_{-k_b} and, respectively, over κ_{k_b} and κ_{-k_b}. In Ref. [39], the EFA has been applied for Skyrme HFB where one-quasiparticle states in the rare-earth region have been studied. It has been shown that the EFA is a reasonable approximation, and it is actually equivalent with the full blocking procedure when the time-odd fields are not taken into account. In the RHB framework, EFA has been also applied in Ref. [82] for the study of odd-A systems by blocking the one-quasiparticle states with the lowest energy in the ground state of the neighboring even system.

Within the EFA, currents are ignored, and the effect of blocking is averaged over the two configurations of the $+K$ and $-K$ subspaces. In this way, at each iteration step of the numerical application, only fields that retain time-reversal symmetry are involved.

The full blocking procedure breaks the time-reversal symmetry and leads to the currents around the symmetry axis in the nuclear medium. Consequently, in a second step, we avoid the EFA for the calculation of isomeric energies and treat the currents in the RHB framework. This can be performed relatively easily by using a cranked RHB code where the cranking axis points in the direction of the symmetry axis (z axis). In this way, axial symmetry is preserved.

The cranking approximation rotating around an axis (x axis) perpendicular to the symmetry axis has been applied either in studies of rotating nuclei and of superdeformed bands [84–88] where the time-reversal symmetry is also broken. In the case of a rotation around the symmetry axis, the cranked RHB equations include the Coriolis operator $\Omega_z \hat{J}_z$, where Ω_z is the rotation frequency and $\hat{J}_z$ is the projection of the total angular momentum on the rotation axis and are written as

$$\begin{pmatrix} \hat{h}_D - \lambda - \Omega_z \hat{J}_z & \hat{\Delta} \\ -\hat{\Delta}^* & -\hat{h}^*_D + \lambda + \Omega_z \hat{J}^*_z \end{pmatrix} \begin{pmatrix} U_k(\boldsymbol{r}) \\ V_k(\boldsymbol{r}) \end{pmatrix} = E_k \begin{pmatrix} U_k(\boldsymbol{r}) \\ V_k(\boldsymbol{r}) \end{pmatrix}. \tag{20}$$

Now, the Dirac Hamiltonian,

$$h_D = \boldsymbol{\alpha}[\boldsymbol{p} - \boldsymbol{V}(\boldsymbol{r})] + V_0(\boldsymbol{r}) + \beta[M + S(\boldsymbol{r})] \tag{21}$$

contains, in addition to the scalar $S(\boldsymbol{r})$ and timelike $V(\boldsymbol{r})$ potentials, the spacelike components of the meson fields,

$$\boldsymbol{V}(\boldsymbol{r}) = g_\omega \boldsymbol{\omega}(\boldsymbol{r}) + g_\rho \tau_3 \boldsymbol{\rho}(\boldsymbol{r}) + e\frac{1-\tau_3}{2}\boldsymbol{A}(\boldsymbol{r}). \tag{22}$$

This last term along with the Coriolis operator are responsible for the breaking of the time-reversal symmetry. In the present paper, we apply this approximation without rotation ($\Omega_z = 0$) for the formation of two-quasiparticle configurations oriented along the z axis where the unpaired nucleons contribute to the formation of currents around the z-axis formation and feed the spacelike components of the meson fields. In the applications discussed in the following, we use this method with breaking of time-reversal symmetry only for the point coupling functional DD-PC1.

III. SINGLE-PARTICLE ENERGIES AND NILSSON DIAGRAMS

One of the basic criteria for K isomers to appear is axial deformation. For nuclei with large axially symmetric deformations, the K-quantum number, i.e., the component of the total angular momentum along the symmetry axis, in principle, does not represent an observable, but it turns out to be a relatively well-conserved quantity (for details, see Refs. [62,89,90]. The ground state of such an even-even nucleus is formed by a configuration with $K = 0$ where the doubly degenerate single-particle orbits with opposite angular momentum along the symmetry axis are equally occupied. The ground state has angular momentum $I = 0$, and the lowest excitations are the members of a rotational band built on this state, connected by very large $E2$ transitions to the ground state. Other excitations are of vibrational character, usually also connected with relatively large transitions. K isomers are two- or multiquasiparticle excitations characterized by the total K quantum number $K = K_1 + K_2 + \cdots$. They form the band heads of rotational bands build on such states, and the angular momentum of such a state is $I = K$. The transition probability of this state to the ground state is, therefore, connected with $\Delta I = K$ and for large values of K such a transition is strongly hindered, causing the long lifetime of such an isomer.

The *intruder* states, i.e., high-j single-particle orbitals belonging originally to the next higher oscillator shell above the valence shell but shifted down into the valence shell by the strong spin-orbit field in nuclei are relatively pure configurations because the different parity does not allow mixing with the orbits in the valence shell. Some of them have high-K values. The occupation of such quasiparticle levels leads to high-K isomers. Therefore, it is evident that the existence, the position, and the lifetime of such isomers is strongly influenced by the single-particle structure in the underlying deformed mean field and by the position of the single-particle states in the corresponding spherical mean field. Phenomenological descriptions, such as the microscopic-macroscopic method based on the Nilsson or a deformed Woods-Saxon potential, can provide a better description of such isomers as compared to the experiment because here the single-particle energies are adjusted to experimental data.

It is well known, that density functional theories, in general, and the nuclear energy density functionals have problems with the description of single-particle energies. In principle, they are no observables in the strict sense and in the original concept of Hohenberg and Kohn [91] one could not even reproduce shell effects. The problem was solved in the framework of Kohn and Sham [92] by introducing an auxiliary single-particle field. In nuclear physics, the spin-orbit splitting has a crucial influence for the shell structure and in all nonrelativistic density functionals [93–95], the spin-orbit force has been adjusted to experimental single-particle energies.

Within the CDF framework, the natural emergence of the spin-orbit coupling, without the need of extra parameters or information from single-particle experimental data, is one of the most important advantages. In earlier studies, this has been shown to provide a good description of the size of spin-orbit splitting in doubly magic nuclei with around 20% deviations in the absolute values from experiment [66,96]. In a more recent study, we were able to show that CDFs give also a good description of the SO splitting in $N = 20$ isotones and of the rapid reduction of the p splitting in ^{34}Si, which is connected with the central density depletion [97]. However, a direct comparison with the experimental single-particle states shows that there is wrong ordering of some of the states as they are calculated within constrained DFT (CDFT), the respective shell gaps are enhanced and in all cases the calculated spectrum is less dense around the Fermi surface. These facts are well known, and, specifically, the last two are associated with the low effective mass of the nucleons in relativistic mean-field approach. Of course, the inclusion of correlations that go beyond the simple mean field have been shown to improve the quality of the description of the spectra. For example, particle vibration coupling (PVC) in covariant theory [98,99] gives a more accurate description of the single-particle states especially in the ^{132}Sn and ^{208}Pb nuclei and improves the quantitative analysis of the reduction of the neutron p splitting in ^{34}Si [97].

In deformed nuclei, PVC has because of the numerical complexity so far only been taken into account in very schematic models. In investigations of the spectroscopic properties of deformed nuclei based on nuclear density functional theory, PVC is usually not taken into account. It is assumed that it can be neglected because part of the correlations are already taken into account by the deformed mean field. Such investigations are to some extent successful [100,101] because they are usually based on the parameter set Skyrme III [102] with a relatively large effective mass $m^*/m = 0.76$ in contrast to the modern successful parameter sets D1S [103] with $m^*/m = 0.67$ or SLy4 [104] with $m^*/m = 0.69$. For the relativistic models DD-ME2 and DD-PC1 used in this investigation, the effective Lorentz masses are also relatively small: $m^*/m = 0.66$. Having this in mind, we have to expect that the resulting single-particle energies in the deformed cases show deviations from the values of Nilsson, which are adjusted to experimental values.

In order to study these phenomena in a more quantitative way, we examine the effect of deformation in the intrinsic scheme of the nucleus [90] by comparing with the well-known Nilsson diagrams [9], which depict the change in single-particle energies with increasing deformation.

The deformation parameter β_2 is a measure of the axial deformation of the nuclear shape and, using the Bohr model [89], it is defined by the quadrupole moment,

$$\langle \hat{Q}_{20} \rangle = \sqrt{\frac{9}{5\pi}} A R_0^2 \beta_2. \tag{23}$$

In the case of self-consistent mean-field calculations, we have the possibility to change the deformation β_2 of the nuclear system we are interested in by solving the RHB equations in an external quadrupole field and constraining the quadrupole moment $\langle \hat{Q}_{20} \rangle$ according to Eq. (23). More specifically, we use the method of a quadratic constraint [62]. In this way, we can determine, for each deformation parameter β_2, the canonical energies $\epsilon_k(\beta_2)$ which are defined as the diagonal elements of the single-particle Hamiltonian $\hat{h}$ in the canonical basis (for details, see Sec. 7.3.2 of Ref. [62]). With this method, we are able to draw diagrams similar to Nilsson diagrams for the nuclear areas where we want to examine the formation of K isomers.

As a typical example for the medium to heavy mass region, we show in Fig. 1 such diagrams for the neutron and proton levels in the nucleus ^{176}Hf with $Z = 72$ and $N = 104$. The deformation parameter β_2 changes from 0 (spherical shape) to 0.5 (prolate shape). In Fig. 2, the corresponding diagrams produced by the original Nilsson model [105] are shown for ^{176}Hf. The model parameters used for the specific deformed region are, for neutrons, $\kappa = 0.0637$ and $\mu = 0.40$ and, for protons, $\kappa = 0.0624$ and $\mu = 0.61$. States with positive parities are given in solid lines, and states with negative parities are given in dashed ones. In the diagrams produced with the RHB model, the change in the Fermi surface is also indicated using a black dashed line, whereas the vertical dotted line corresponds to the deformation of the ground state of the nucleus ^{176}Hf.

At zero deformation, the orbits are characterized by the spherical quantum numbers $n\ell j$ provided next to the points that correspond to the respective degenerate orbits. Of special interest are the single-particle states that start from the intruder states ($1i_{13/2}$ for the neutrons and $1h_{11/2}$ for the protons). These intruder orbits belong to the next higher major oscillator

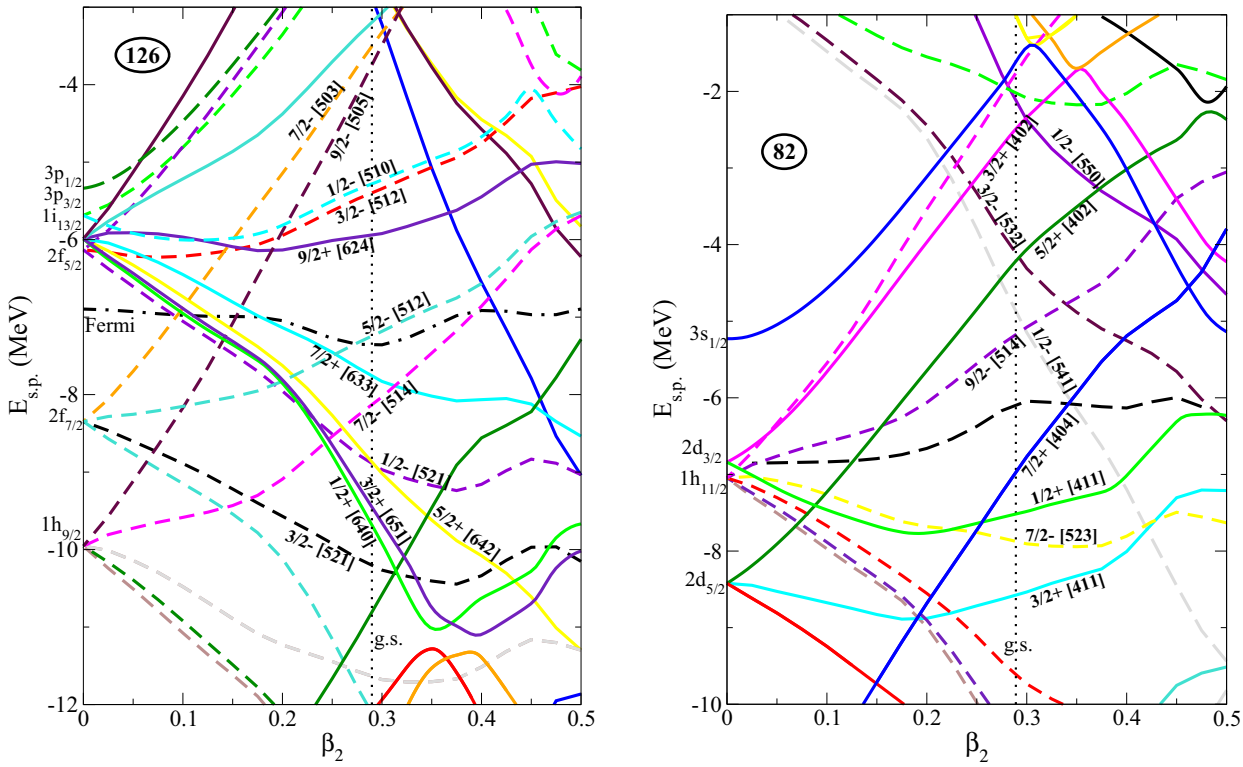

(a) Neutron states (b) Proton states

FIG. 1. Nilsson diagram for neutrons and protons close to the Fermi surface in ^{176}Hf obtained with the relativistic functional DD-ME2.

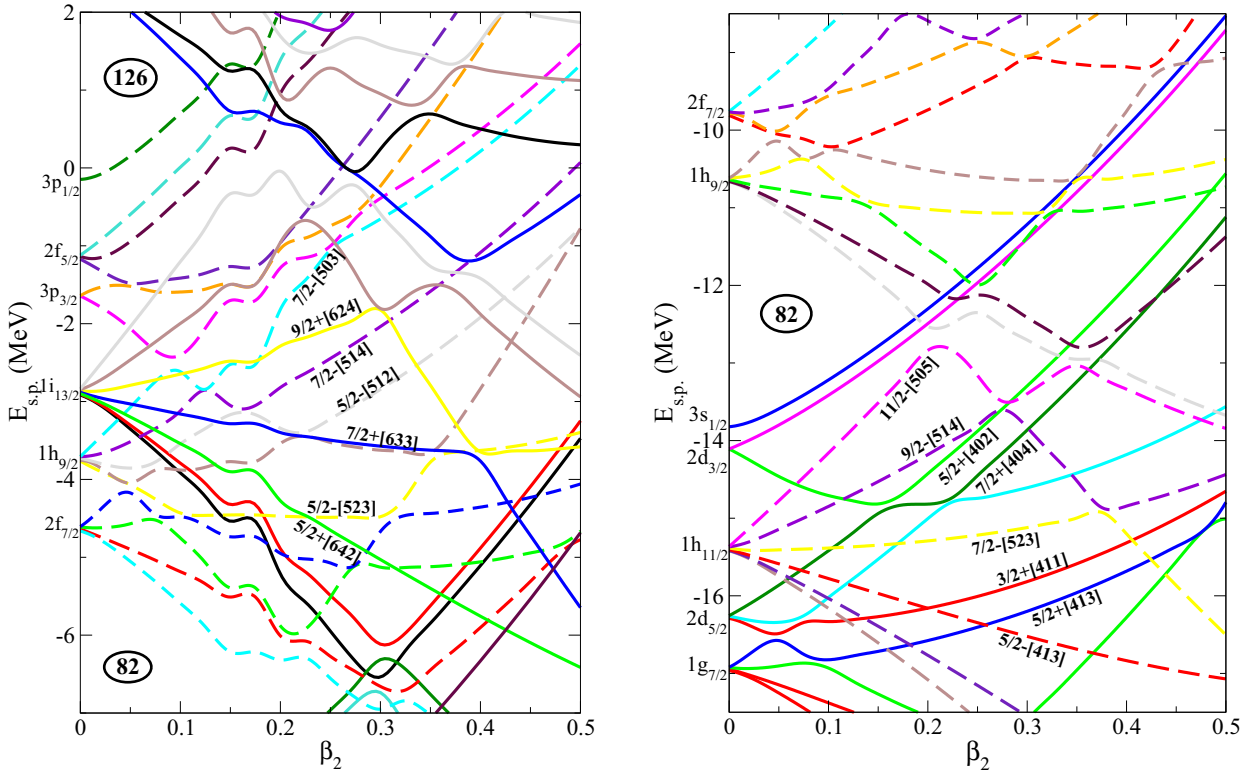

(a) Neutron states (b) Proton states

FIG. 2. Nilsson diagram for neutrons and protons with the Nilsson model.

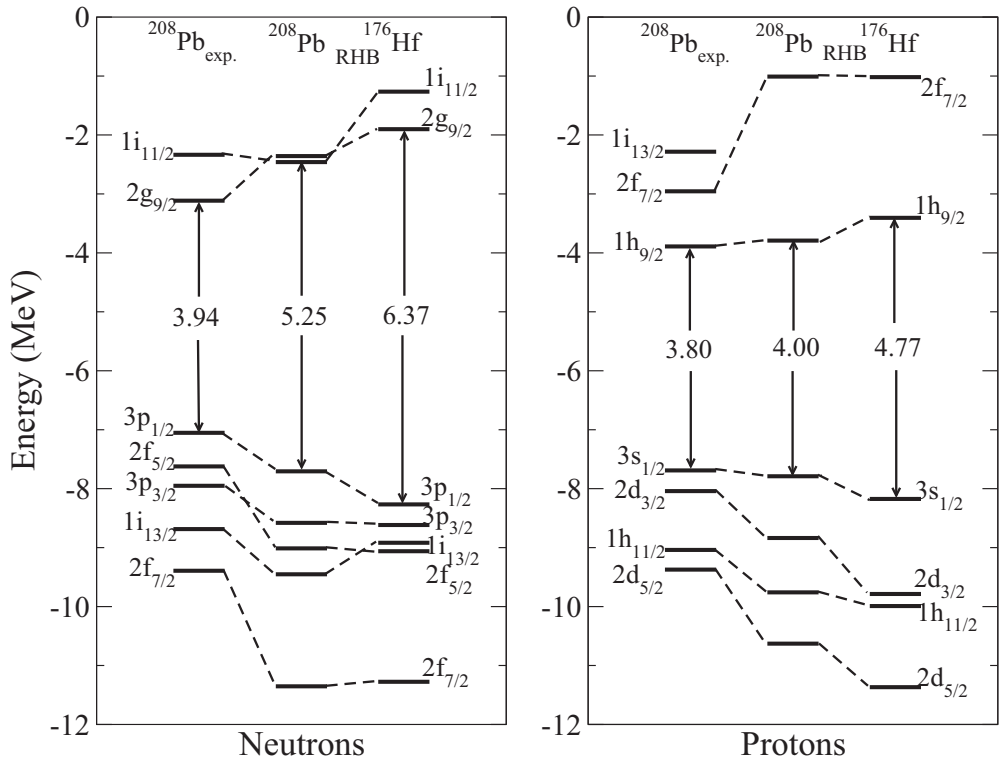

FIG. 3. Single-particle energies of neutron and proton states for the spherical nucleus ^{208}Pb and the nucleus ^{176}Hf with enforced spherical shape. In both diagrams, the first column corresponds to the experimental energies of ^{208}Pb, the second and third states calculated with the RHB model.

shell above the valence shell, they are shifted down by the strong spin-orbit coupling, and their parities are opposite to that of the valence shell. Using the quadratic constraint on the quadrupole moment, we can force ^{176}Hf to obtain a spherical shape. This is not a mean-field equilibrium solution, but it is used as a starting point where we can see the initial positions of the single-particle states. We can compare these states with the experimentally observed single-particle states of the doubly magic nucleus ^{208}Pb given by the excitation spectrum of neighboring odd nuclei. A schematic of this comparison is shown in Fig. 3. For both neutron and proton diagrams, the first column shows the experimental states of ^{208}Pb, and the third column shows the states of ^{176}Hf at zero deformation where we have shifted the spectrum so that the middle of the shell gap is at the same energy with the middle of the experimental gap. Additionally, we have included calculations of the single-particle states of ^{208}Pb with the DD-ME2 functional in the second column. In Fig. 3, we observe the different ordering of the neutron states between the data and the theoretical calculations in addition to a more dense experimental spectrum.

As the deformation increases, each spherical orbit is divided in $j + 1/2$ separate states. For large deformations, the single-particle states are characterized by the asymptotic Nilsson quantum numbers or Nilsson labels $K\pi[Nn_z\Lambda]$. The identification of the states near the Fermi surface for the ground state of ^{176}Hf by their Nilsson labels in Fig. 1 shows that states with high j's come closer energetically. The same can be seen in the diagrams of the actual Nilsson model where the Nilsson labels of the same states around the same deformations 0.2 and 0.3 are given. As expected, there are some qualitative differences between the two models. First, as in Fig. 3, there is different ordering of the neutron spherical orbits between the Nilsson and the RHB model. Second, the Nilsson model leads to a more dense spectrum with more states present in the 9-MeV interval of the diagrams, which is connected with the larger shell gaps within the RHB model. Furthermore, the shift of the states with respect to deformation is more steep in the RHB diagrams, also contributing to a less dense spectrum at a given deformation. Nevertheless, in both cases, the same $K\pi[Nn_z\Lambda]$ states with high j are present in an energy window of up to 4 MeV at the same neutron and proton numbers and around $\beta_2 = 0.3$ deformation.

As a result of these investigations, we see clearly, that, as expected by the arguments given above, there are essential differences between the self-consistently determined single-particle energies in Fig. 1 and the Nilsson energies adjusted to experimental data in Fig. 2. We, therefore, cannot expect that the results for the K isomers presented in the following sections will show a similar agreement with experimental data as those obtained on the basis of Nilsson energies.

However, we have to emphasize that using universal density functionals has still some advantages as compared to the microscopic-macroscopic method: First of all, the fact that the CDFT-method is universal, one can expect a higher predictive power in other areas of the nuclear chart, in particular, far from the valley of stability or for extremely heavy nuclei where one has no experimental knowledge of the single-particle levels

TABLE I. Common two-quasiparticle configurations used as building blocks for K-isomer formation in prolate deformed nuclei in the region of medium to heavy nuclei as in Ref. [5].

Neutrons	Protons
$Z \approx 70$–74 $N \approx 100$–108	
6^-:$5/2^-[512]$, $7/2^+[633]$	
6^+:$5/2^-[512]$, $7/2^-[514]$	
6^+:$5/2^+[642]$, $\mathbf{7/2^+[633]}$	6^+:$5/2^+[402]$, $7/2^+[404]$
8^-:$9/2^+[624]$, $7/2^-[514]$	8^-:$9/2^-[514]$, $7/2^+[404]$

in this region, in particular, in cases where intruder states from higher unknown shells could be important. Second, there is hope to improve the single-particle energies in covariant density functionals: (i) by including particle-vibrational coupling in deformed nuclei, (ii) by taking into account tensor forces [106] which are known to have a strong influence on the position of single-particle energies [107,108], and (iii) by considering in future *ab initio* density functionals derived from the scattering data. There is work in this direction [72]. However, applications in deformed nuclei are connected with considerable numerical difficulties and have to be left for the future.

In Table I, the most common two-quasiparticle configurations that appear in the specific region are presented as in Ref. [5], together with the constituent combination of states that lead to their creation.

IV. THE EFFECT OF PAIRING

Before we go on and calculate the systematic appearance of specific isomers in the Hf isotopes and in $N = 104, 106$ isotones, we want to examine the effect of pairing correlations in the calculation of a test case. The nucleus ^{176}Hf has been chosen because with $N = 104$ is in the middle of the $N = 82$–126 neutron shell.

It has been shown in Ref. [109] that relativity has practically no influence on pairing phenomena in nuclei because they are determined by the orbits in close vicinity to the Fermi surface. Orbits in the Dirac sea are more then 1200 MeV away and have because of the strongly dropping uv coefficients, basically no influence in the gap equation. The scale of pairing effects (determined by pp correlations) of several MeV is well separated from the scale of the binding energies (determined by ph correlations) of several hundreds of MeV. Therefore, there is no reason to use, in Eq. (5), the same effective force in the functional $E_{\rm RMF}$ for the ph and in the functional $E_{\rm pair}$ for the pp channel. In fact, it has been shown in Ref. [80] that pairing correlations derived from the meson-exchange forces (strongly attractive in the scalar and nearly as strongly repulsive in the vector channel) lead to completely nonphysical results. Therefore, we follow Ref. [77] and use a hybrid model with a nonrelativistic effective pairing force motivated by the Brink-Booker part of the well-known Gogny force [110],

$$V^{pp}(1,2) = \sum_{i=1,2} e^{-(r_1-r_2)/\mu_i{}^2} \times (W_i + B_i P^\sigma - H_i P^\tau - M_i P^\sigma P^\tau), \quad (24)$$

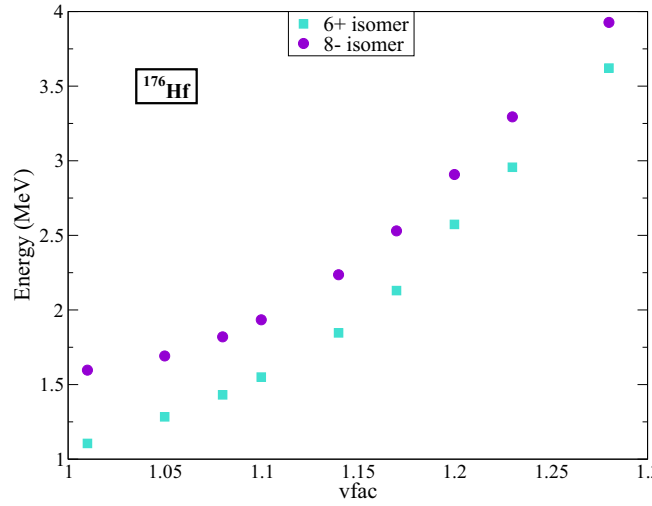

FIG. 4. Change in the 6^+ and 8^- isomers energy with respect to pairing strength using the DDME2 force. The pairing force (26) is multiplied with the factor $V_{\rm fac}$.

with the set D1S [110] for the parameters μ_i, W_i, B_i, H_i, and M_i $(i = 1, 2)$. The advantage of this force is that, due to its finite range, it does not require the introduction of an artificial pairing cutoff to avoid the divergences at high momenta.

This method has been very successful, but it requires substantial computational efforts, in particular, in deformed nuclei. Therefore, an alternative pairing force has been developed by Tian *et al.* in Ref. [78], the TMR force separable in momentum space. It contains two parameters which are adjusted to reproduce the pairing properties of the Gogny force in the $^1S_0$ channel of neutron matter. In this channel, the gap equation reads

$$\Delta(k) = -\int_0^\infty \frac{k'^2 dk'}{2\pi^2} \langle k|V^{^1S_0}|k'\rangle \frac{\Delta(k')}{2E(k')}, \quad (25)$$

and the pairing force TMR is separable in momentum space,

$$\langle k|V^{^1S_0}|k'\rangle = -Gp(k)p(k'). \quad (26)$$

The two parameters determining this force are the strength G and the range α that goes in the Gaussian ansatz $p(k) = e^{-\alpha^2 k^2}$. Their values have been adjusted to $G = 728$ MeV fm^3 and $\alpha = 0.644$ fm in order to reproduce the density dependence of the gap at the Fermi surface, calculated with the D1S parametrization of the Gogny force [103].

In the following, we show the influence of this pairing force with varying strength on a test example. Since in what follows, we will be concentrating on the 6^+ and 8^- systematic appearance in an isotopic and an isotonic chain we study, here, these cases. In the ^{176}Hf nucleus, the first isomer is constructed by the two-quasiparticle configuration $\nu 5/2^-[512] \otimes \nu 7/2^-[514]$ and the second isomer by the configuration $\pi 9/2^-[514] \otimes \pi 7/2^+[404]$.

In Fig. 4, we show the results of this calculation. We have used the DD-ME2 functional increasing the pairing strength in the channel of the blocked configuration, whereas we have kept the original value in the other channel. So, for the 6^+

isomer, neutron pairing is enhanced, and for the 8^- isomer, proton pairing is enhanced. For larger values of the enhancement parameter, we have, for both cases, an increase in the isomeric energy. This was to be expected since stronger pairing leads to an increase in the binding energy of the ground state, which, in turn, means that the formation of the isomer via breaking of the respective pairs of nucleons requires more energy.

This short examination illustrates how one can, in principle, use the excitation energy of K isomers to adjust the pairing strength. This method could be an alternative to the use of odd-even mass differences, or the moments of inertia in the case of rotating nuclei as has been performed in a fine-tuning of the rotational spectra within cranked RHB theory [88] because the original strength of the Gogny is to slightly too large, for example, in the $A \approx 250$ mass region. However, in the rest of our calculations, we have kept the pairing force of Ref. [78] with the constants G and α given after Eq. (26) in order to have a systematic evaluation of the framework used to construct 2qp K-isomer energies and not just obtain a fine-tuned reproduction of the experimental results.

V. RESULTS

In our calculation, the 2qp states are determined by blocking the lowest neutron or proton quasiparticle orbitals located in the vicinity of the Fermi energy that corresponds to the fully paired ground-state solution. After performing the iterative minimization, the energy of the two-quasiparticle excitation is obtained as the difference between the energy of the self-consistent blocked RHB solution and the energy of the fully paired equilibrium minimum.

A. The 6^+ isomer in Hf isotopes and in $N = 104$ isotones

In this section, we present the systematics of the 6^+ high-K isomeric state in the even-even Hf isotopes with neutron number $98 \leqslant N \leqslant 108$ and in the $N = 104$ isotones with atomic number $68 \leqslant Z \leqslant 84$. The 2qp configurations that form a 6^+ isomer (according to Table I and Fig. 1) are as follows: $\nu 5/2^-[512] \otimes \nu 7/2^-[514]$ and $\nu 5/2^+[642] \otimes \nu 7/2^+[633]$ for neutrons and $\pi 5/2^+[402] \otimes \pi 7/2^+[404]$ for protons. This is in line with the configuration assignment given in Refs. [5,63] and in the nuclear data table [3] for the six isotopes $^{170-180}$Hf and the isotones $N = 104$ from ^{172}Er to ^{180}Os.

1. Hf isotopes

The formation of isomers in well-deformed nuclei occurs when nucleons fill high-K orbitals coming close to the Fermi surface, and the projections of their total angular momentum can couple to a large total value K, parallel to the symmetry axis. The excitation energy is roughly equal to the energy cost of breaking the respective pairs or equivalently equal to the sum of the quasiparticle energies E_k, i.e.,

$$E^* \approx \sum_k \sqrt{(\epsilon_k - \lambda)^2 + \Delta_k^2} = \sum_k E_k, \qquad (27)$$

where $\epsilon_k = h_{k,k}$ and $\Delta_k = \Delta_{k,-k}$ are the single-particle energy and the pairing gap in the canonical basis. λ is the Fermi energy. Therefore, the position of the lowest quasiparticle orbitals in the ground state of each nucleus under consideration provides information about the possible formation of low-energy two-quasiparticle states. In Fig. 5, we show the position of the quasiparticle states with energy less than 3 MeV for neutrons [Fig. 5(a)] and protons [Fig. 5(b)] in the even-even $^{170-180}$Hf isotopes calculated with the relativistic density functional DD-ME2. In the neutron spectrum of Fig. 5(a), we see that the Fermi surface moves to higher energies with increasing neutron number. Here, the neutron high-j orbitals that are candidates to form a low-lying 6^+ state are the 2qp configurations: $\nu 5/2^+[642] \otimes \nu 7/2^+[633]$ and $\nu 5/2^-[512] \otimes \nu 7/2^-[514]$. We observe, in Fig. 1, that the relative energy difference $|\epsilon_k - \lambda|$ of the two orbitals $\nu 5/2^+[642]$ and $\nu 7/2^+[633]$ forming a 6^+_ν state increases gradually with neutron number and, thus, the sum of the two quasiparticle energies $\sum E_k$ of that state will increase. The relative position of the neutron orbitals $\nu 5/2^-[512]$ and $\nu 7/2^-[514]$ that create an alternative 6^+ isomer displays a different pattern. For the isotopes of $^{170-176}$Hf their relative energy difference decreases gradually whereas around $^{178-180}$Hf an abrupt raise shows up. Figure 6 displays the interplay between the excitation energies of these two quasineutron configurations $\nu 5/2^+[642] \otimes \nu 7/2^+[633]$ (black line) and $\nu 5/2^-[512] \otimes \nu 7/2^-[514]$ (red line). As we observe, the $\nu 5/2^+[642] \otimes \nu 7/2^+[633]$ configuration is the lowest-lying 2qp state for the isotopes of ^{170}Hf and ^{172}Hf with excitation energy $\approx$1.9 and 1.7 MeV, respectively, whereas in ^{174}Hf and ^{176}Hf, the favored configuration is $\nu 5/2^-[512] \otimes \nu 7/2^-[514]$ with energies 1.5 and 1 MeV, respectively. In ^{178}Hf and ^{180}Hf, both neutron configurations are calculated at excitation energies higher than 4 MeV. For these isotopes, the 6^+ configuration favored by our model appears to be a 2qp state formed by two protons as discussed below.

In Fig. 5(b), we show the structure of the proton quasiparticle spectrum for the $^{170-180}$Hf isotopes. Since the number of protons is constant, the relative position of the Fermi surface remains almost unchanged. Here, the lowest-lying 6^+ two-quasiproton state corresponds to the configuration $\pi 5/2^+[402] \otimes \pi 7/2^+[404]$ as shown in Fig. 6 (green line). The excitation energy of 6^+_π occurs at around 2.6 to 2.7 MeV in all the isotopes $^{170-180}$Hf under consideration.

In Fig. 7, the evaluation of the lowest-lying 6^+ 2qp states in $^{170-180}$Hf isotopes are compared to data. Purple dots correspond to the DD-ME2 functional with EFA, filled turquoise squares correspond to the DD-PC1 functional with EFA, and open turquoise squares correspond to the calculation with the DD-PC1 functional allowing for breaking of time-reversal symmetry. The data taken from Refs. [3,63] are shown as black crosses. In $^{170-172}$Hf isotopes, the excitation energies correspond to the two-quasineutron configuration $\nu 5/2^+[642] \otimes \nu 7/2^+[633]$, in $^{174-176}$Hf to $\nu 5/2^-[512] \otimes \nu 7/2^-[514]$, and in $^{178-180}$Hf to the two-quasiproton configuration $\pi 5/2^+[402] \otimes \pi 7/2^+[404]$. This is different from the configuration assignment in the review of the experimental energies in Ref. [3] where the $\pi 5/2^+[402] \otimes \pi 7/2^+[404]$ configuration is assigned to the 6^+ isomer in $^{170-180}$Hf with

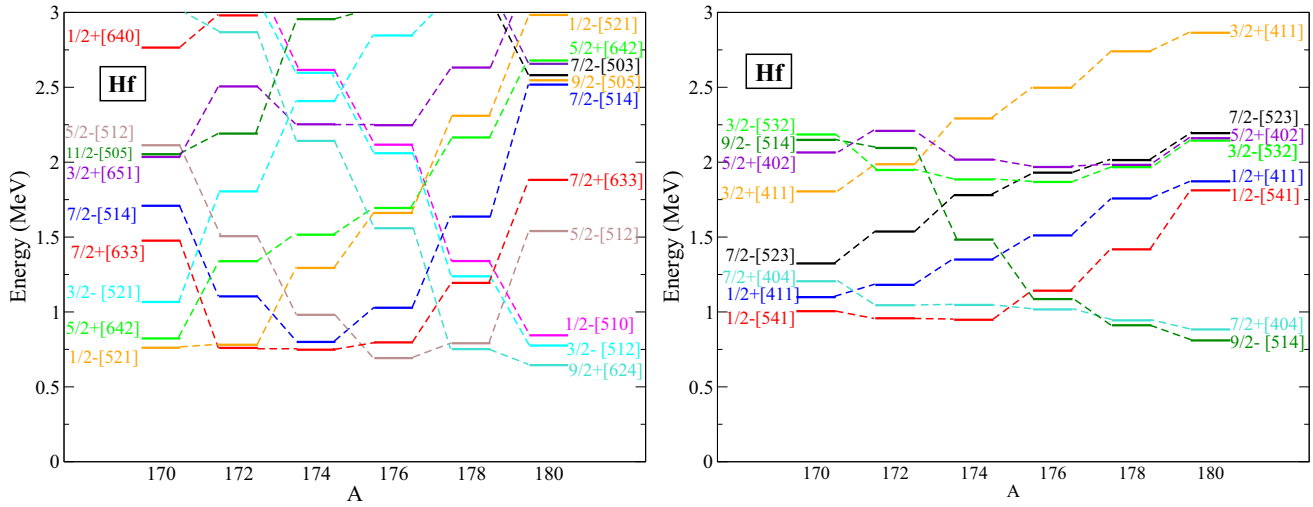

(a) Quasineutron energies (b) Quasiproton energies

FIG. 5. Quasiparticle energies in even-even Hf isotopes with neutron number $170 \leqslant A \leqslant 180$ obtained with the relativistic functional DD-ME2 and the separable pairing force TMR of Eq. (26).

the case of ^{176}Hf showing an admixture with $\nu 5/2^-[512] \otimes \nu 7/2^-[514]$.

In general, the calculated lowest energies follow the trend of the experimental values. Quantitatively, the two functionals give similar results with the DD-PC1 functional predicting slightly higher excitation energies for $^{170-176}$Hf and slightly lower values for $^{178-180}$Hf. The inclusion of currents leads, in each isotope, to a decreasing in the excitation energy by roughly 0.3 MeV. The calculated excitation energies that correspond to the two-quasineutron configuration reproduce more accurately the experimental data. In the $^{178-180}$Hf isotopes where the lowest-lying 6^+ state originates from the two-quasiproton configuration, the difference between our theoretical calculations and the experimental assignments is approximately 1 MeV. Table II includes the results of the lowest-lying 6^+ isomeric states in comparison with data. The first column contains the calculations with the DD-ME2 functional, in the second column are calculations with the DD-PC1, and in the third column are calculations with the DD-PC1 functional and with the inclusion of time-reversal symmetry breaking. In the last column, the experimental data are shown.

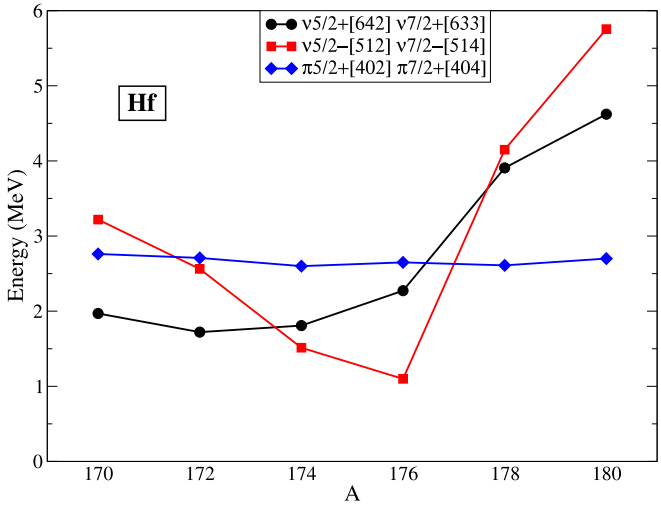

FIG. 6. Excitation energies of the 6^+ 2qp states coming from the configurations $\nu 5/2^+[642] \otimes \nu 7/2^+[633]$ (black dots), $\nu 5/2^-[512] \otimes \nu 7/2^-[514]$ (red squares), and $\pi 5/2^+[402] \otimes \pi 7/2^+[404]$ (blue diamonds) in the $^{170-180}$Hf isotopes calculated with the relativistic functional DD-ME2 and the separable TRM pairing force.

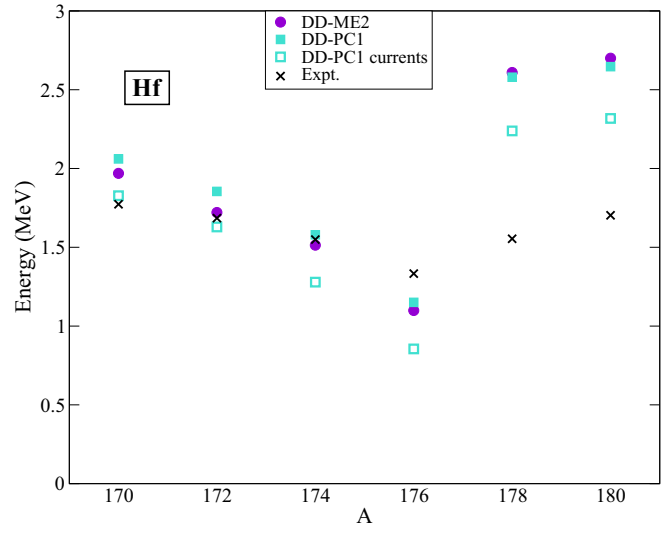

FIG. 7. Excitation energy of the 6^+ 2qp states in $^{170-180}$Hf isotopes obtained with the relativistic functionals DD-ME2 (purple dots) and DD-PC1 (turqoise squares) and the separable pairing force TMR. Results with the inclusion of currents using the DD-PC1 functional are shown in turqoise open squares. Calculations are compared to the data [3,63].

TABLE II. The 6^+ excitation energy in $^{170-180}$Hf calculated with the relativistic functionals DD-ME2 (first column), DD-PC1 (second column), and DD-PC1 with time-reversal symmetry breaking (third column). In all cases, the separable pairing force TMR has been used. Experimental data [3,63] are given in column four.

	DD-ME2	DD-PC1	DD-PC1 + currents	Expt.
^{170}Hf	1.969	2.061	1.827	1.773
^{172}Hf	1.721	1.855	1.629	1.685
^{174}Hf	1.513	1.579	1.279	1.549
^{176}Hf	1.099	1.151	0.855	1.333
^{178}Hf	2.610	2.579	2.239	1.554
^{180}Hf	2.700	2.647	2.318	1.703

2. $N = 104$ *isotones*

In this section, the formation of the 6^+ high-K isomer is studied in the five even-even $N = 104$ isotones with $68 \leqslant Z \leqslant 76$. The dominant high-$j$ orbitals from which this 2qp state originates are $\nu 5/2^-[512]$ and $\nu 7/2^-[514]$. In Fig. 8, we show the quasiparticle energies up to 3 MeV of the neutron orbitals in the $N = 104$ isotones with $172 \leqslant A \leqslant 180$ calculated with the DD-ME2 functional. The relative energy difference between the two orbitals increases gradually from 1.2 to 1.7 MeV. Figure 9 displays the evolution of the excitation energy for the 6^+ high-K isomer in the $N = 104$ isotones with $172 \leqslant A \leqslant 180$. Purple dots correspond to the DD-ME2 functional, filled turquoise squares correspond to the DD-PC1 functional, and open turquoise squares correspond to calculation with the DD-PC1 functional with the inclusion of time-reversal symmetry breaking. The data taken from Refs. [3,63] are shown as black crosses. We observe that, qualitatively, we reproduce the trend of the data with the exception of ^{176}Hf where the data exhibit a downward kink probably because of the strong mixing with an alternative two-quasiproton 6^+ state as suggested in Ref. [63]. Calculations with the DD-ME2

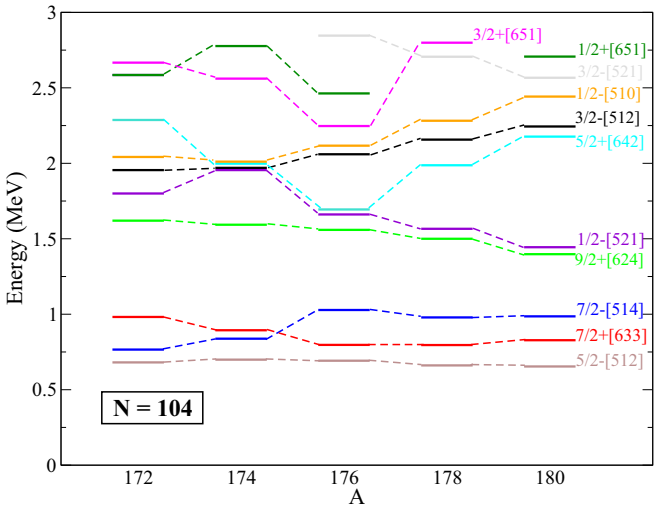

FIG. 8. The same as Fig. 5(a) but for $N = 104$ isotones with $172 \leqslant A \leqslant 180$.

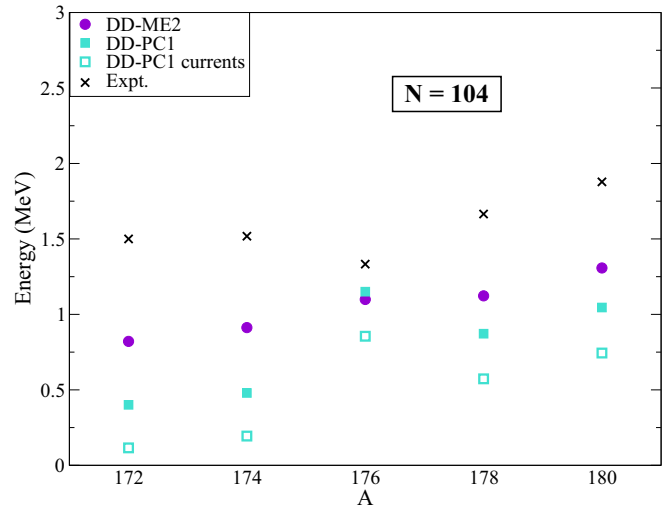

FIG. 9. The same as Fig. 6 but for $N = 104$ isotones with $172 \leqslant A \leqslant 180$.

functional reproduce better the data except from ^{176}Hf where the DD-PC1 functional gives a better description. Results with the inclusion of time-reversal symmetry breaking lead to a constant decrease in roughly 0.3 MeV in the excitation energies of all isotones in the chain.

Table III includes the evaluation of the excitation energy of the 6^+ state in the $N = 104$ isotones with $172 \leqslant A \leqslant 180$. The first column contains the calculations with the DD-ME2 functional, in the second column are calculations with the DD-PC1, and in the fourth column are calculations with the DD-PC1 functional and with the inclusion of time-reversal symmetry breaking. In the last column, the experimental data are shown.

B. 8^- isomer in Hf isotopes and in $N = 106$ isotones

1. *Hf isotopes*

Another case of a systematically occurring high-Kisomer is the 8^- two-quasiparticle excitation that has been observed experimentally (see Ref. [3]) in the $^{170-184}$Hf isotopes. This particular isomer originates from the two-quasiproton configuration: $\pi 9/2^-[514] \otimes \pi 7/2^+[404]$.

Figure 10 is the same as Fig. 5(b) but extended up to ^{186}Hf to include the neutron quasiparticle energies of all nuclei in which an 8^- isomer occurs. We observe that the $\pi 9/2^-[514]$ orbital (dark green line) has a relatively high-quasiparticle

TABLE III. The same as Table II for the 6^+ excitation energy formed by the $\nu 5/2^-[512] \otimes \nu 7/2^-[514]$ 2qp configuration in $N = 104$ isotones with $172 \leqslant A \leqslant 180$.

	DD-ME2	DD-PC1	DD-PC1 currents	Expt.
172 Er	0.821	0.401	0.116	1.5
174 Yb	0.913	0.479	0.194	1.518
176 Hf	1.099	1.151	0.855	1.333
178 W	1.123	0.872	0.573	1.665
180 Os	1.308	1.046	0.744	1.878

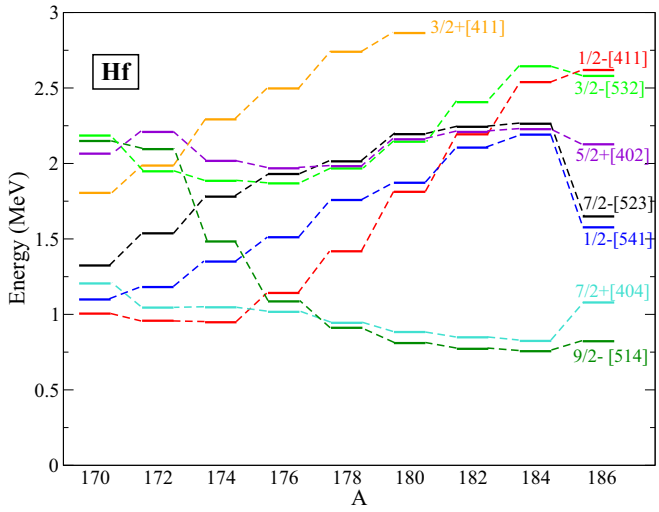

FIG. 10. The same as Fig. 5(b) but for the isotopic chain $^{170-186}$Hf.

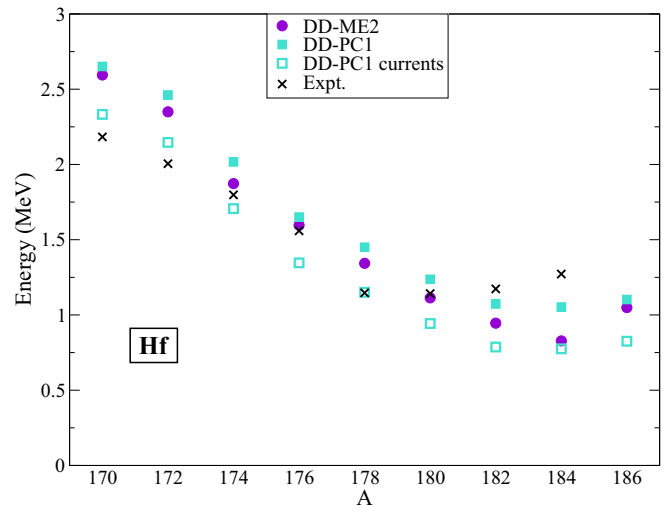

FIG. 11. The same as Fig. 6 but for the 8^- 2qp states in the isotopic chain $^{170-186}$Hf.

energy at nearly 2.3 MeV in ^{170}Hf. The orbital approaches the Fermi level and eventually becomes the lowest-quasiparticle state in ^{178}Hf up to ^{186}Hf. The second orbital of the configuration $\pi 7/2^+[404]$ (turquoise line) has a very low-quasiparticle energy throughout the isotopic chain, exhibiting only a slight decrease from the initial value of 1.4 MeV in ^{170}Hf.

Applying the blocking approximation to the two quasineutron states we can examine how the energy of the 8^- isomer evolves along the isotopic chain. Table IV includes the evaluated excitation energy for each isotope calculated with the functionals DD-ME2 and DD-PC1 and compared to experimental data [3]. In Fig. 11, the results of Table IV are schematically presented.

Comparing the results in Fig. 11 with the proton quasiparticle energies in Fig. 10, the calculated excitation energy of the 8^- 2qp state follows the trend of the two proton orbitals $\pi 9/2^-[514]$ and $\pi 7/2^+[404]$ which also explains the evolution of the experimentally observed excitation energies. The experimentally observed excitation energies start at 2.183 MeV for ^{170}Hf and decrease linearly losing about 0.2 MeV at each subsequent isotope, until ^{180}Hf where they reach a minimum and then increase for the two last nuclei ^{184}Hf and ^{186}Hf. Our calculations predict the 8^- excitation energy at around $\approx$2.5 MeV in ^{170}Hf and gradually lose energy approaching the data. The difference is that the minimum appears in ^{184}Hf and not in ^{180}Hf as in the experiment. The result in ^{186}Hf was included to show that ^{184}Hf is the theoretical minimum. The two functionals give similar results, and the inclusion of currents has the same effect of giving 0.3-MeV lower energy.

TABLE IV. The same as Table II for the excitation energy of the 8^- 2qp state formed by the configurations $\pi 9/2^-[514] \otimes \pi 7/2^+[404]$ in the isotopic chain $^{170-186}$Hf.

	DD-ME2	DD-PC1	DD-PC1 currents	Expt.
170 Hf	2.595	2.651	2.333	2.183
172 Hf	2.350	2.461	2.146	2.005
174 Hf	1.873	2.017	1.707	1.798
176 Hf	1.596	1.651	1.346	1.559
178 Hf	1.343	1.450	1.151	1.147
180 Hf	1.113	1.237	0.943	1.142
182 Hf	0.945	1.073	0.787	1.173
184 Hf	0.827	1.053	0.775	1.272
186 Hf	1.049	1.103	0.826	

2. $N = 106$ *isotones*

In this section, the 8^- isomeric state in the $N = 106$ isotones with atomic number $68 \leqslant Z \leqslant 82$ is studied. In this isotonic chain, not all nuclei are axially deformed since ^{184}Pt is a transitional nucleus, ^{186}Hg exhibits oblate-prolate shape coexistence, and ^{188}Pb is a rather neutron-deficient nucleus. Nevertheless, an 8^- isomer was experimentally observed in Ref. [63]. The configuration of the two neutron orbitals that create the particular isomer is s follows: $\nu 7/2^-[514] \otimes \nu 9/2^+[624]$.

In Fig. 12, the quasiparticle energies of the neutron orbitals with energies less than 3 MeV in the $N = 106$ isotones from Er to Pb calculated with the DD-ME2 functional are presented. The $\nu 7/2^-[514]$ orbital corresponds to the orange line, and the $\nu 9/2^+[624]$ orbital corresponds to the turquoise one. We observe that the relative energy difference of the two orbitals is constantly increasing with proton number from Er to Os (with the exception of ^{176}Yb where the energy is almost the same as in ^{174}Er) and, then, remains stable from Pt to Pb.

In Fig. 13 and Table V, the calculation of our model for the 8^- excitation energy in the above-mentioned isotonic chain are presented in comparison to data. We observe that our theoretical calculations reproduce qualitatively the behavior of the data from ^{174}Er to ^{182}Os which are, indeed, the axially symmetric nuclei of the chain. However, quantitatively, our calculations overpredict the data by about 0.8–1 MeV. The calculated excitation energy is $\approx$1.9 MeV in ^{174}Er and increases to 2.3 to 2.4 MeV in ^{182}Os. For the last three nuclei

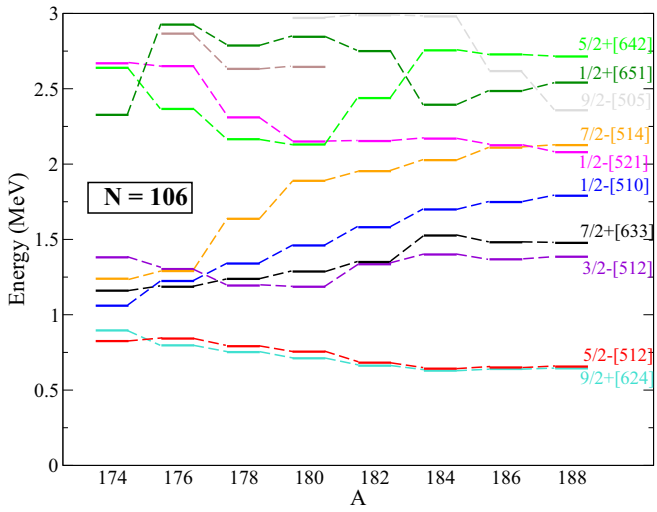

FIG. 12. The same as Fig. 8 but for $N = 106$ isotones with $174 \leqslant A \leqslant 188$.

(Pt to Pb), the evaluated excitation energy remains almost unchanged, in contrast to the experimental values. The calculations between the DD-ME2 and the DD-PC1 functionals are equivalent, whereas the inclusion of currents affects all the resulting energies by 0.3 MeV.

In Table VI, we show the effective β_2 deformation parameter calculated within our model for both DD-ME2 and DD-PC1 functionals. As we can see, there is no significant change between the ground state and the corresponding 8^- state, both being of prolate shape with the isomeric state having a slightly larger β_2 value in all cases.

VI. OVERVIEW AND CONCLUSIONS

In this paper, we have used the self-consistent mean-field approach within the relativistic Hartree-Bogoliubov framework based on relativistic energy density functionals to calculate the two-quasiparticle excitations in heavy nuclei with axially deformed shapes. Throughout this paper, we used the meson-exchange functional DD-ME2 and the point coupling functional DD-PC1 both with density depended coupling constants. Well-established experimental data of the systematic appearance of 6^+ and 8^- low-energy high-K isomers in the region of Er to Pb ($68 \leqslant Z \leqslant 84$, $98 \leqslant N \leqslant 112$) and in nuclei with $A \approx 160$–190 were used for the evaluation of our method. The theoretical calculation of the corresponding excitation energies is based on the blocking approximation. The application of this approximation in the theoretical framework is implemented in two different ways. First, the time-reversal symmetry of the unblocked state is preserved by the EFA. Second, the time-reversal symmetry is broken, and the induced currents coming from the unpaired blocked nucleons are taken into account in the calculation of the fields.

As a first step, using calculations with a quadrupole constraint, we constructed Nilsson diagrams within the canonical basis of the RHB framework for the case of ^{176}Hf. We were, thus, able to demonstrate that, in axially deformed nuclei in the region of interest, several neutron and proton orbitals with high-K values come close to the Fermi surface.

Satisfying this basic property, our next step was to examine the effect of pairing correlations using the 6^+ and 8^- 2qp states in ^{176}Hf as a test case. It was shown that, as the pairing strength increases, so does the excitation energy. This is

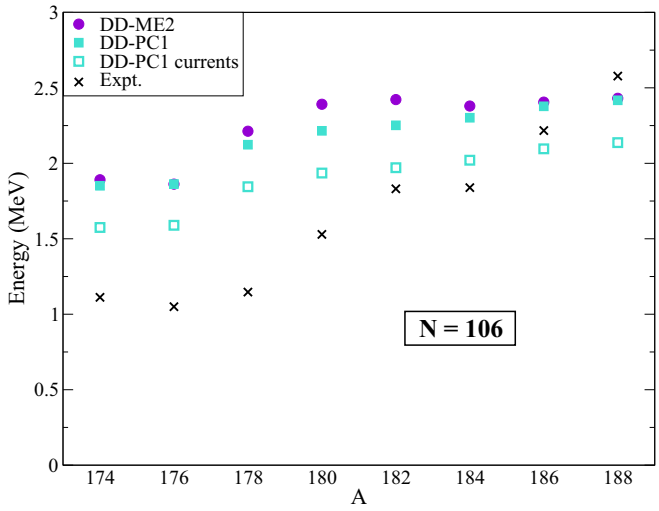

FIG. 13. The same as Fig. 11 but for $N = 106$ isotones with $174 \leqslant A \leqslant 188$.

TABLE V. The same as Table II for the excitation energy of the 8^- state formed by the $\nu 7/2^-[514] \otimes \nu 9/2^+[624]$ 2qp configuration in $N = 106$ isotones with $172 \leqslant A \leqslant 188$.

	DD-ME2	DD-PC1	DD-PC1 currents	Expt.
174 Er	1.891	1.851	1.575	1.112
176 Yb	1.862	1.863	1.589	1.050
178 Hf	2.213	2.123	1.845	1.147
180 W	2.391	2.215	1.935	1.529
182 Os	2.422	2.252	1.971	1.831
184 Pt	2.380	2.302	2.020	1.839
186 Hg	2.405	2.378	2.096	2.217
188 Pb	2.431	2.418	2.137	2.578

TABLE VI. The effective deformation parameter β_2 in the ground state and in the $\nu 7/2^-[514] \otimes \nu 9/2^+[624]$ state of the $N = 106$ nuclei with the DD-ME2 and DD-PC1 parameter sets.

	DDME2		DD-PC1	
	g.s.	8^-	g.s.	8^-
174 Er	0.322	0.329	0.324	0.330
176 Yb	0.318	0.325	0.318	0.326
178 Hf	0.288	0.295	0.292	0.302
180 W	0.285	0.300	0.293	0.307
182 Os	0.300	0.311	0.303	0.314
184 Pt	0.306	0.315	0.306	0.315
186 Hg	0.297	0.305	0.299	0.308
188 Pb	0.291	0.302	0.293	0.305

expected since the amount of energy needed to break a pair of nucleons is larger for stronger pairing. This result shows that one could use the strength of pairing to fine-tune the calculation of the excitation energy in order to reproduce the experimental data in a better way. However, in this paper, the strength of the TMR separable pairing force was always set to its default value.

In the main part of this paper, our microscopic self-consistent approach, provides a good qualitative description of the systematic appearance of the 6^+ and 8^- high-K isomers in the nuclear chains under consideration. This is true for both DD-ME2 and DD-PC1 functionals since they show equivalent results. The detailed examination of the underlying quasiparticle structure demonstrates its importance in the resulting excitation energy of high-K isomers. More specifically, the fact that the isomer energy is, to a first approximation, equal to the sum of the individual quasiparticle energies, provides an explanation of the trend followed by the experimental values in each nuclear chain. Furthermore, the 2qp configuration assignment for the creation of the 6^+ isomer in $N = 104$ and the 8^- isomer in Hf isotopes and $N = 106$ isotones agrees with the assignment given in Ref. [3]. There is, however, a difference in the configurations leading to the lowest 6^+ isomer in the Hf isotopes: In the case of ^{178,180}Hf, it originates from the $\pi 5/2^+[402] \otimes \pi 7/2^+[404]$ configuration whereas, in the isotopes $^{170-176}$Hf, the configurations $\nu 5/2^-[512] \otimes \nu 7/2^-[514]$ and $\nu 5/2^+[642] \otimes \nu 7/2^+[633]$ are the ones with the lowest energy within our model.

On a quantitative level, our results reproduce well the experimental values of the excitation energies in most cases. It is important to note that, for the DD-PC1 functional, the full blocking scheme with the inclusion of currents via the breaking of time-reversal symmetry provides a standard effect in the final excitation energies. Namely, in all cases, it gives an extra binding of about 0.3 MeV in the 2qp state lowering by the same amount the corresponding excitation energy.

For a future work, one could consider the inclusion of correlations beyond the mean field, that might provide a better qualitative description. An example could be the particle-vibration coupling that has been shown to provide a better picture of the single-particle structure around the Fermi surface in spherical nuclei [97,98]. A more ambitious task is to develop a method of calculating the lifetimes of the proposed isomers by analyzing the rotational spectra of the nuclear ground states and finding possible deexcitation paths. Finally, the fact that, in the case of $N = 106$ isotones, high-K isomers exist in the last four nuclei that are transitional or shape coexisting shows an interesting connection. A further theoretical examination can be achieved in our framework by using multidimensional constraint calculations and investigating the energy surface of both ground and two-quasiparticle states.

ACKNOWLEDGMENTS

The work of K.E.K. was financed within the Tenure Track Pilot Programme of the Croatian Science Foundation and the École Polytechnique Fédérale de Lausanne, and the Project No. TTP-2018-07-3554 Exotic Nuclear Structure and Dynamics with funds of the Croatian-Swiss Research Programme. V.P.'s research was conducted within the Call Fellowship for Postodoctoral research implemented by the University of Thessaly and funded by the Stavros Niarchos Foundation. P.R. was supported by the DFG cluster of excellence "Origins" [111]. Important assistance has been provided by the IT Center of Aristotle University of Thessaloniki for accessing the computational hub of HellasGrid.

[1] A. K. Jain, B. Maheshwari, S. Garg, M. Patial, and B. Singh, Nucl. Data Sheets **128**, 1 (2015).
[2] K. Heyde and J. L. Wood, Rev. Mod. Phys. **83**, 1467 (2011).
[3] F. G. Kondev, G. D. Dracoulis, and T. Kibédi, At. Data Nucl. Data Tables **103**, 50 (2015).
[4] P. M. Walker and F. R. Xu, Phys. Scr. **91**, 013010 (2016).
[5] G. D. Dracoulis, P. M. Walker, and F. G. Kondev, Rep. Prog. Phys. **79**, 076301 (2016).
[6] D. Ackermann, Nucl. Phys. A **944**, 376 (2015).
[7] D. Ackermann and C. Theisen, Phys. Scr. **92**, 083002 (2017).
[8] P. Walker and Z. Podolyak, Phys. Scr. **95**, 044004 (2020).
[9] S. G. Nilsson, Kong. Dan Vid. Sel. Mat. Fys Med. **19N16**, 1 (1955).
[10] A. Bohr, B. R. Mottelson, and D. Pines, Phys. Rev. **110**, 936 (1958).
[11] S. T. Belyaev, Mat. Fys. Medd. Dan. Vid. Selsk. **31**, 11 (1959).
[12] K. Jain, O. Burglin, G. Dracoulis, B. Fabricius, N. Rowley, and P. Walker, Nucl. Phys. **A591**, 61 (1995).
[13] G. Dracoulis, F. Kondev, and P. Walker, Phys. Lett. B **419**, 7 (1998).
[14] C. J. Gallagher and S. A. Moszkowski, Phys. Rev. **111**, 1282 (1958).
[15] C. J. Gallagher, Phys. Rev. **126**, 1525 (1962).
[16] K. Jain, P. Walker, and N. Rowley, Phys. Lett. B **322**, 27 (1994).
[17] F. Kondev, G. Dracoulis, A. Byrne, T. Kibédi, and S. Bayer, Nucl. Phys. A **617**, 91 (1997).
[18] F. R. Xu, P. M. Walker, J. A. Sheikh, and R. Wyss, Phys. Lett. B **435**, 257 (1998).
[19] W. Nazarewicz, M. Riley, and J. Garrett, Nucl. Phys. A **512**, 61 (1990).
[20] V. M. Strutinsky, Nucl. Phys. A **95**, 420 (1967).
[21] F. R. Xu, R. Wyss, and P. M. Walker, Phys. Rev. C **60**, 051301 (1999).
[22] F. R. Xu, P. M. Walker, and R. Wyss, Phys. Rev. C **62**, 014301 (2000).
[23] F. R. Xu, E. G. Zhao, R. Wyss, and P. M. Walker, Phys. Rev. Lett. **92**, 252501 (2004).
[24] H. L. Liu, F. R. Xu, S. W. Xu, R. Wyss, and P. M. Walker, Phys. Rev. C **76**, 034313 (2007).
[25] H. L. Liu, F. R. Xu, P. M. Walker, and C. A. Bertulani, Phys. Rev. C **83**, 011303 (2011).
[26] H. L. Liu, F. R. Xu, P. M. Walker, and C. A. Bertulani, Phys. Rev. C **83**, 067303 (2011).
[27] Y. Shi, F. R. Xu, P. M. Walker, and G. D. Dracoulis, Phys. Rev. C **85**, 064304 (2012).

[28] Y. Shi, P. M. Walker, and F. R. Xu, Phys. Rev. C **85**, 027307 (2012).
[29] H. L. Liu and F. R. Xu, Phys. Rev. C **87**, 067304 (2013).
[30] H. L. Liu, P. M. Walker, and F. R. Xu, Phys. Rev. C **89**, 044304 (2014).
[31] Z. J. Bai, C. F. Jiao, Y. Gao, and F. R. Xu, Chin. Phys. C **40**, 094102 (2016).
[32] P. Jachimowicz, M. Kowal, and J. Skalski, Phys. Rev. C **92**, 044306 (2015).
[33] P. Jachimowicz, M. Kowal, and J. Skalski, Phys. Rev. C **98**, 014320 (2018).
[34] M. Palczewski, P. Jachimowicz, and M. Kowal, arXiv:2006.02245.
[35] S. Ćwiok, J. Dobaczewski, P.-H. Heenen, P. Magierski, and W. Nazarewicz, Nucl. Phys. A **611**, 211 (1996).
[36] S. Ćwiok, W. Nazarewicz, and P. H. Heenen, Phys. Rev. Lett. **83**, 1108 (1999).
[37] T. Duguet, P. Bonche, and P.-H. Heenen, Nucl. Phys. A **679**, 427 (2001).
[38] M. Bender, P. Bonche, T. Duguet, and P.-H. Heenen, Nucl. Phys. A **723**, 354 (2003).
[39] N. Schunck, J. Dobaczewski, J. McDonnell, J. Moré, W. Nazarewicz, J. Sarich, and M. V. Stoitsov, Phys. Rev. C **81**, 024316 (2010).
[40] M. Bender and P.-H. Heenen, J. Phys.: Conf. Ser. **420**, 012002 (2013).
[41] Y. Shi, J. Dobaczewski, and P. T. Greenlees, Phys. Rev. C **89**, 034309 (2014).
[42] L. Bonneau, P. Quentin, N. Minkov, D. Ivanov, J. Bartel, H. Molique, and M. H. Koh, Bulg. J. Phys. **46**, 366 (2019).
[43] J. L. Egido and L. M. Robledo, Phys. Rev. Lett. **85**, 1198 (2000).
[44] J.-P. Delaroche, M. Girod, H. Goutte, and J. Libert, Nucl. Phys. A **771**, 103 (2006).
[45] M. Warda and J. L. Egido, Phys. Rev. C **86**, 014322 (2012).
[46] V. Prassa, B.-N. Lu, T. Nikšić, D. Ackermann, and D. Vretenar, Phys. Rev. C **91**, 034324 (2015).
[47] A. K. Rath, P. M. Walker, C. R. Praharaj, and F. R. Xu, Int. J. Mod. Phys. E **15**, 1653 (2006).
[48] S. K. Ghorui and C. R. Praharaj, Eur. Phys. J. A **54**, 163 (2018).
[49] C. R. Praharaj, S. Bhoi, Z. Naik, S. K. Ghorui, and S. K. Patra, arXiv:1904.01229.
[50] P. Ring and H. J. Mang, Phys. Rev. Lett. **33**, 1174 (1974).
[51] H. B. Jeppesen, R. M. Clark, K. E. Gregorich, A. V. Afanasjev, M. N. Ali, J. M. Allmond, C. W. Beausang, M. Cromaz, M. A. Deleplanque, I. Dragojevic, J. Dvorak, P. A. Ellison, P. Fallon, M. A. Garcia, J. M. Gates, S. Gros, I. Y. Lee, A. O. Macchiavelli, S. L. Nelson, H. Nitsche, L. Stavsetra, F. S. Stephens, and M. Wiedeking, Phys. Rev. C **80**, 034324 (2009).
[52] B.-H. Li, Z.-H. Zhang, and Y.-A. Lei, Chin. Phys. C **37**, 014101 (2013).
[53] Z.-H. Zhang, Phys. Rev. C **98**, 034304 (2018).
[54] X.-T. He and Y.-C. Li, Phys. Rev. C **98**, 064314 (2018).
[55] X.-T. He, S.-Y. Zhao, Z.-H. Zhang, and Z.-Z. Ren, Chinese Physics C **44**, 034106 (2020).
[56] X.-T. He and Z.-L. Chen, Chin. Phys. C **43**, 064106 (2019).
[57] K. Hara and Y. Sun, Int. J. Mod. Phys. E **4**, 637 (1995).
[58] Y.-C. Yang, Y. Sun, S.-J. Zhu, M. Guidry, and C.-L. Wu, J. Phys. G: Nucl. Part. Phys. **37**, 085110 (2010).
[59] F.-Q. Chen, Y.-X. Liu, Y. Sun, P. M. Walker, and G. D. Dracoulis, Phys. Rev. C **85**, 024324 (2012).
[60] F.-Q. Chen, Y. Sun, P. M. Walker, G. D. Dracoulis, Y. R. Shimizu, and J. A. Sheikh, J. Phys. G: Nucl. Part. Phys. **40**, 015101 (2013).
[61] L.-J. Wang, F.-Q. Chen, T. Mizusaki, M. Oi, and Y. Sun, Phys. Rev. C **90**, 011303 (2014).
[62] P. Ring and P. Schuck, *The Nuclear Many-Body Problem* (Springer-Verlag, Berlin, 1980).
[63] G. D. Dracoulis, G. J. Lane, F. G. Kondev, A. P. Byrne, R. O. Hughes, P. Nieminen, H. Watanabe, M. P. Carpenter, R. V. F. Janssens, T. Lauritsen, D. Seweryniak, S. Zhu, P. Chowdhury, and F. R. Xu, Phys. Lett. B **635**, 200 (2006).
[64] S. K. Tandel, P. Chowdhury, F. G. Kondev, R. V. F. Janssens, T. L. Khoo, M. P. Carpenter, T. Lauritsen, C. J. Lister, D. Seweryniak, S. Zhu, A. Deacon, S. J. Freeman, N. J. Hammond, G. D. Jones, E. F. Moore, and J. F. Smith, Phys. Rev. C **94**, 064304 (2016).
[65] B. D. Serot and J. D. Walecka, Adv. Nucl. Phys. **16**, 1 (1986).
[66] P. Ring, D. Vretenar, and B. Podobnik, Nucl. Phys. A **598**, 107 (1996).
[67] D. Vretenar, A. V. Afanasjev, G. A. Lalazissis, and P. Ring, Phys. Rep. **409**, 101 (2005).
[68] *Lecture Notes in Physics*, edited by G. A. Lalazissis, P. Ring, and D. Vretenar (Springer-Verlag, Heidelberg, 2004), Vol. 641.
[69] T. D. Cohen, R. J. Furnstahl, and D. K. Griegel, Phys. Rev. Lett. **67**, 961 (1991).
[70] A. V. Afanasjev and P. Ring, Phys. Rev. C **62**, 031302 (2000).
[71] U. Hofmann and P. Ring, Phys. Lett. B **214**, 307 (1988).
[72] S. H. Shen, H. Z. Liang, W. H. Long, J. Meng, and P. Ring, Prog. Part. Nucl. Phys. **109**, 103713 (2019).
[73] G. A. Lalazissis, T. Nikšić, D. Vretenar, and P. Ring, Phys. Rev. C **71**, 024312 (2005).
[74] T. Nikšić, D. Vretenar, and P. Ring, Phys. Rev. C **78**, 034318 (2008).
[75] P. W. Zhao, Z. P. Li, J. M. Yao, and J. Meng, Phys. Rev. C **82**, 054319 (2010).
[76] X. Roca-Maza, X. Viñas, M. Centelles, P. Ring, and P. Schuck, Phys. Rev. C **84**, 054309 (2011).
[77] T. Gonzalez-Llarena, J. L. Egido, G. A. Lalazissis, and P. Ring, Phys. Lett. B **379**, 13 (1996).
[78] Y. Tian, Z. Y. Ma, and P. Ring, Phys. Lett. B **676**, 44 (2009).
[79] Y. Tian, Z. Y. Ma, and P. Ring, Phys. Rev. C **80**, 024313 (2009).
[80] H. Kucharek and P. Ring, Z. Phys. A **339**, 23 (1991).
[81] T. Nikšić, N. Paar, D. Vretenar, and P. Ring, Comput. Phys. Commun. **185**, 1808 (2014).
[82] L. Li, J. Meng, P. Ring, E.-G. Zhao, and S.-G. Zhou, Chin. Phys. Lett. **29**, 042101 (2012).
[83] S. Perez-Martin and L. M. Robledo, Phys. Rev. C **78**, 014304 (2008).
[84] W. Koepf and P. Ring, Nucl. Phys. A **511**, 279 (1990).
[85] J. König and P. Ring, Phys. Rev. Lett. **71**, 3079 (1993).
[86] A. V. Afanasjev, J. König, and P. Ring, Phys. Rev. C **60**, 051303(R) (1999).
[87] A. Afanasjev, P. Ring, and J. König, Nucl. Phys. A **676**, 196 (2000).
[88] A. V. Afanasjev, T. L. Khoo, S. Frauendorf, G. A. Lalazissis, and I. Ahmad, Phys. Rev. C **67**, 024309 (2003).

[89] A. Bohr and B. R. Mottelson, *Nuclear Structure Volume I: Single-Particle Motion* (W. A. Benjamin, New York/Amsterdam, 1969).
[90] J. A. Sheikh, J. Dobaczewski, P. Ring, L. M. Robledo, and C. Yannouleas, arXiv:1901.06992.
[91] P. Hohenberg and W. Kohn, Phys. Rev. **136**, B864 (1964).
[92] W. Kohn and L. J. Sham, Phys. Rev. **140**, A1133 (1965).
[93] D. Vautherin and D. M. Brink, Phys. Rev. C **5**, 626 (1972).
[94] J. Dechargé and D. Gogny, Phys. Rev. C **21**, 1568 (1980).
[95] M. Baldo, P. Schuck, and X. Viñas, Phys. Lett. B **663**, 390 (2008).
[96] M. Bender, K. Rutz, P.-G. Reinhard, J. A. Maruhn, and W. Greiner, Phys. Rev. C **60**, 034304 (1999).
[97] K. Karakatsanis, G. A. Lalazissis, P. Ring, and E. Litvinova, Phys. Rev. C **95**, 034318 (2017).
[98] E. Litvinova and P. Ring, Phys. Rev. C **73**, 044328 (2006).
[99] E. V. Litvinova and A. V. Afanasjev, Phys. Rev. C **84**, 014305 (2011).
[100] J. Libert and P. Quentin, Phys. Rev. C **25**, 571 (1982).
[101] J. Libert, M. Meyer, and P. Quentin, Phys. Rev. C **25**, 586 (1982).
[102] M. Beiner, H. Flocard, N. Van Giai, and P. Quentin, Nucl. Phys. A **238**, 29 (1975).
[103] J. F. Berger, M. Girod, and D. Gogny, Comput. Phys. Commun. **63**, 365 (1991).
[104] E. Chabanat, P. Bonche, P. Haensel, J. Meyer, and R. Schaeffer, Nucl. Phys. A **635**, 231 (1998).
[105] S. G. Nilsson, C.-F. Tsang, A. Sobiczewski, Z. Szymanski, S. Wycech, C. Gustafson, I.-L. Lamm, P. Moller, and B. Nilsson, Nucl. Phys. A **131**, 1 (1969).
[106] W. H. Long, P. Ring, N. Van Giai, and J. Meng, Phys. Rev. C **81**, 024308 (2010).
[107] G. A. Lalazissis, S. Karatzikos, M. Serra, T. Otsuka, and P. Ring, Phys. Rev. C **80**, 041301 (2009).
[108] S. Shen, H. Liang, J. Meng, P. Ring, and S. Zhang, Phys. Rev. C **97**, 054312 (2018).
[109] M. Serra and P. Ring, Phys. Rev. C **65**, 064324 (2002).
[110] J. F. Berger, M. Girod, and D. Gogny, Nucl. Phys. A **428**, 23 (1984).
[111] www.origins-cluster.de.